Amorphous-crystalline dual-layer structures resulting from metastable liquid phase separation in $(Fe_{50}Co_{25}B_{15}Si_{10})_{80}Cu_{20}$ melt-spun ribbons*

Cao Chong-De(曹崇德)[a)†], Gong Su-Lian(弓素莲)[a)], Guo Jin-Bo(郭晋波)[a)], Song Rui-Bo(宋瑞波)[a)], Sun Zhan-Bo(孙占波)[b)], Yang Sen(杨 森)[b)], and Wang Wei-Min(王伟民)[c)]

[a)] *Department of Applied Physics, Northwestern Polytechnic University, Xi'an* 710072, *China*

[b)] *School of Science, Xi'an Jiaotong University, Xi'an* 710049, *China*

[c)] *Scool of Materials Science and Engineering, Shandong University, Ji'nan* 250061, *China*

(Received 28 December 2011; revised manuscript received 5 March 2012)

$(Fe_{50}Co_{25}B_{15}Si_{10})_{80}Cu_{20}$ ribbons are prepared by using the single-roller melt-spinning method. A dual-layer structure consisting of a (Fe, Co)-rich amorphous phase and a Cu-rich crystalline phase forms due to metastable liquid phase separation before solidification. The magnetic hysteresis loops of the as-quenched and annealed samples are measured at room temperature. It is indicated that the coercivity of the ribbon is almost zero in the as-quenched state. The crystallization leads to the increase of coercivity and decrease of saturation magnetization.

Keywords: amorphous alloy, rapid solidification, liquid phase separation, magnetic property

PACS: 61.50.Ah, 64.75.Op, 75.60.Ej, 81.70.Pg **DOI:** 10.1088/1674-1056/21/8/086102

1. Introduction

The development of metallic glass matrix composites has attracted much interest due to the unique structures and properties in comparison with conventional metallic glasses.[1−4] By means of rapid solidification, composites can be obtained through the nearly simultaneous occurrence of liquid phase separation and amorphous phase formation, such as La–Zr–Al–Ni–Cu[5] and Fe–Zr–B–Cu.[6]

It is well known that the Fe–Cu and Co–Cu systems are characterized by a large positive heat of mixing and Fe–Co-based alloys with B and Si have negative heat of mixing. Therefore, Fe–Cu,[7] Co–Cu,[8−10] and Fe–Co–Cu[11−13] alloys undergo metastable liquid separation in the undercooling state. Fe–Co–B–Si alloy is a typical metallic glass material.[14] It was reported that the metallic glass matrix composites containing an *in situ* formed ductile crystalline phase were prepared in Fe–Cu[15] and Co–Cu-based alloys.[16] In these alloys, Cu plays an important role in increasing the density of crystal nuclei and forming liquid phase separation. During quenching, metastable liquid phase separation occurs, followed by a liquid-to-glass transition happening in the liquid region. Eventually a composite with amorphous phase forms. Fe-based metallic glasses are promising soft magnetic materials for many electrical devices.[17−20] And $Fe_{50}Co_{25}B_{15}Si_{10}$ has been used as the magnetic function carrier.[21] It is expected to *in-situ* synthesize a kind of composite characterized by good soft magnetic property as well as high electrical conductivity.

In the present study, we present the amorphous-crystalline dual-layer structures and magnetic properties of $(Fe_{50}Co_{25}B_{15}Si_{10})_{80}Cu_{20}$ melt-spun ribbons.

2. Experiment procedures

$(Fe_{50}Co_{25}B_{15}Si_{10})_{80}Cu_{20}$ and $Fe_{50}Co_{25}B_{15}Si_{10}$ ingots were prepared from pure Cu (99.999%), pure Co (99.99%), pure Si (99.9999%), and $Fe_{44.6}B_{55.4}$ alloy in an arc-melting furnace. Melt-spun ribbons were prepared from the ingots by the conventional single-roller melt-spinning method in Ar atmosphere. The $(Fe_{50}Co_{25}B_{15}Si_{10})_{80}Cu_{20}$ ribbons and the

*Project supported by the National Natural Science Foundation of China (Grant Nos. 51171152 and 50871088), the Foundation for Fundamental Research of Northwestern Polytechnic University, China (Grant No. JC201268), and the Fund of the State Key Laboratory of Solidification Processing, China (Grant No. SKLSP201202).

†Corresponding author. E-mail: caocd@nwpu.edu.cn

© 2012 Chinese Physical Society and IOP Publishing Ltd

$Fe_{50}Co_{25}Si_{10}B_{15}$ ribbons were annealed at 873 K for 15 min and 2 h in a tubular furnace with a purified argon atmosphere.

An X-ray diffractometer (XRD, PANalytical B.V. X'Pert Pro using Cu–K radiation), an optical microscope (OM, Zeiss Axio Imager A1m) and a scanning electron microscope (SEM, Zeiss Supra 55) were employed to examine the structures of the melt-spun ribbons. The thermal properties of the ribbons were measured by a Netzsch STA449C differential scanning calorimeter (DSC) in Ar atmosphere. The magnetic hysteresis loops were measured by a Lake Shore 7300 vibrating sample magnetometer (VSM).

3. Results and discussion

Figure 1 shows the XRD patterns of the free surface and the roller surface of $(Fe_{50}Co_{25}B_{15}Si_{10})_{80}Cu_{20}$ ribbon, together with that of $Fe_{50}Co_{25}Si_{10}B_{15}$ ribbon. The XRD pattern of $Fe_{50}Co_{25}B_{15}Si_{10}$ ribbon does not show sharp diffraction peaks but two broad diffuse peaks near $2\theta = 23°$ and $2\theta = 45°$, which indicate that the main structure of the sample is in an amorphous state. The XRD patterns of both the free surface and roller surface of the $(Fe_{50}Co_{25}B_{15}Si_{10})_{80}Cu_{20}$ melt-spun ribbon show sharp diffraction peaks corresponding to the fcc (Cu) crystalline phase. However, it is evident that amorphous phase forms at the roller surface of the $(Fe_{50}Co_{25}B_{15}Si_{10})_{80}Cu_{20}$ melt-spun ribbon. The XRD patterns also reveals that Fe_3Si, Fe_5Si_3, and Fe_2Si intermetallic compound phases possibly form on both sides. The intensity of the peaks of the fcc (Cu) crystalline phase at the roller surface is slightly lower than that at the free surface. The position of the broad peak overlaps that of the fcc peak of (Cu) (111) at approximately $2\theta = 45°$, while the position is similar to that of the $Fe_{50}Co_{25}B_{15}Si_{10}$ ribbon.

Figure 2 shows the DSC curves of the $(Fe_{50}Co_{25}B_{15}Si_{10})_{80}Cu_{20}$ and $Fe_{50}Co_{25}B_{15}Si_{10}$ melt-spun ribbons at a heating rate of 10 K/min. It is found that only one crystallization peak at 813 K for $(Fe_{50}Co_{25}B_{15}Si_{10})_{80}Cu_{20}$ ribbon, whereas there are three peaks at 823 K and near 848 K for $Fe_{50}Co_{25}B_{15}Si_{10}$ ribbon. The first peak for both alloys should correspond to the formation of α-Fe solid solution phase. It can be inferred that the last two peaks on the $Fe_{50}Co_{25}B_{15}Si_{10}$ DSC curve are attributed to the formation of Fe_3Si, Fe_5Si_3 or other intermetallic compound phases during heating. These phases form in the $(Fe_{50}Co_{25}B_{15}Si_{10})_{80}Cu_{20}$ ribbon during quenching.

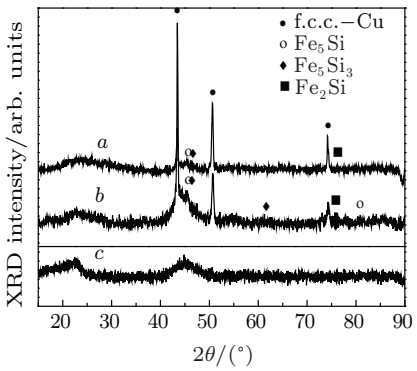


Fig. 1. The X-ray diffraction patterns for as-quenched $(Fe_{50}Co_{25}B_{15}Si_{10})_{80}Cu_{20}$ and $Fe_{50}Co_{25}B_{15}Si_{10}$ melt-spun ribbons: the curve a is the free surface of $(Fe_{50}Co_{25}B_{15}Si_{10})_{80}Cu_{20}$; the curve b is the roller surface of $(Fe_{50}Co_{25}Si_{10}B_{15})_{80}Cu_{20}$; and the curve c is the $Fe_{50}Co_{25}B_{15}Si_{10}$ (reference).

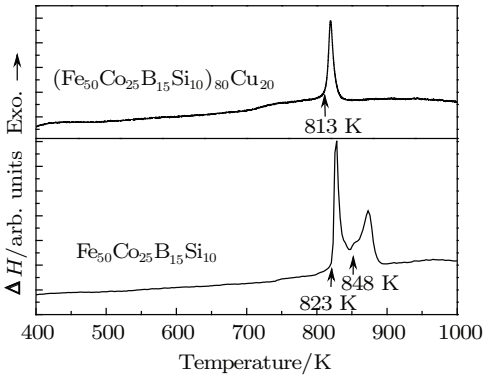


Fig. 2. DSC curves of the $(Fe_{50}Co_{25}B_{15}Si_{10})_{80}Cu_{20}$ and $Fe_{50}Co_{25}B_{15}Si_{10}$ melt-spun ribbons.

Figure 3(a) clearly exhibits a dual-layer structure of $(Fe_{50}Co_{25}B_{15}Si_{10})_{80}Cu_{20}$ melt-spun ribbon. The free surface and the roller surface are marked by arrows. There exists a distinct interface between the two layers. According to energy-dispersive X-ray (EDX) analysis, the average compositions of the free surface layer and the roller surface layer are $Fe_{19}Co_{11}Cu_{61}Si_9$ and $Fe_{48}Co_{23}Cu_{18}Si_{11}$, respectively. The EDX analysis indicates that the roller surface layer is enriched with (Fe, Co), while the free surface layer is enriched with Cu. The interface between the two layers is more clearly present in the SEM image in Fig. 3(b). It can be observed that multi-scale Cu-rich globules from nanometer order to micrometer order are dispersed in the matrix of the (Fe, Co)-rich layer. The size of the nano globule is usually controlled by the alloy composition and cooling rate. Nano-and/or multi-scale

globule with a perfectly spherical morphology could effectively improve the mechanical properties of metallic glass.[22] The formation of the dual-layer structure and an emulsion structure indicates that multi-step liquid phase separation has taken place.

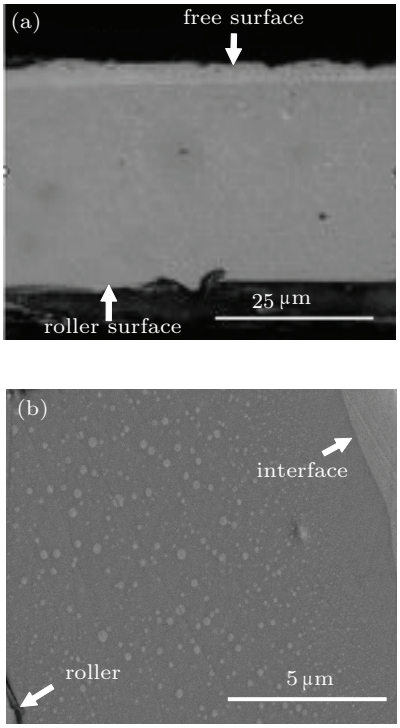


Fig. 3. (colour online) OM (a) and SEM (b) images showing microstructures of the cross section of $(Fe_{50}Co_{25}B_{15}Si_{10})_{80}Cu_{20}$ melt-spun ribbon.

Figure 4 shows the magnetic hysteresis loop of $(Fe_{50}Co_{25}B_{15}Si_{10})_{80}Cu_{20}$ ribbons in the as-quenched state at room temperature. The inset displays the enlarged curve near the central area. The ribbon exhibits a large magnetisability. The saturation magnetization M_s of the $(Fe_{50}Co_{25}B_{15}Si_{10})_{80}Cu_{20}$ ribbon reaches 118.98 emu/g, and the magnetization can achieve saturation at a very low external field. From the inset, it can be observed that the coercivity H_c is very low and the residual magnetization M_r is almost zero. This indicates the ribbon shows a tendency toward static soft magnetic properties with good performances. The $Fe_{50}Co_{25}B_{15}Si_{10}$ ribbon obviously may exhibit a superior soft magnetic property. It has been confirmed that Fe-based metallic alloys containing Cu and Nb could form very small grain microstructures above the crystallization temperature.[23] In the present work the material does not show the deterioration of magnetic properties but the improvement of magnetic properties. The commonly useful parameters of magnetic properties can be relatively figured.[24]

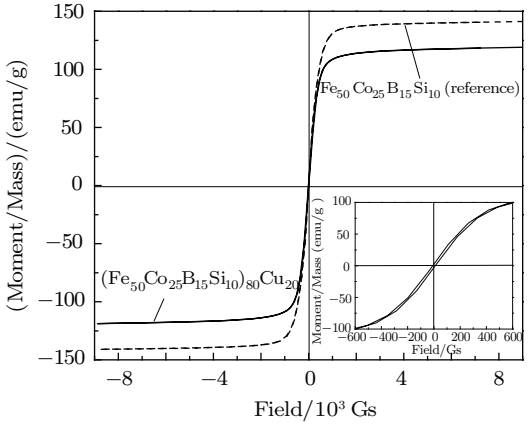


Fig. 4. The magnetic hysteresis loops of the $(Fe_{50}Co_{25}B_{15}Si_{10})_{80}Cu_{20}$ ribbon and $Fe_{50}Co_{25}B_{15}Si_{10}$ ribbon. The inset is for an enlarged section in the vicinity of the origin of the $(Fe_{50}Co_{25}B_{15}Si_{10})_{80}Cu_{20}$ ribbon (1 Gs = 10^{-4} T).

Figure 5 shows the room temperature magnetic hysteresis loops of $(Fe_{50}Co_{25}B_{15}Si_{10})_{80}Cu_{20}$ ribbons annealed at 873 K for different times. The longer the annealing time, the lower the value of M_s is. It is obviously noted that the annealing temperature is much higher than the starting crystallization temperature. During annealing, the formation of Fe-based intermetallic compounds possibly reduces the volume fraction of magnetic phases, thereby leading to the decrease of M_s. Figure 5 also indicates that annealing significantly increases H_c and therefore, soft magnetic properties are deteriorated. On the other hand, H_c changes little for different annealing times (15 min and 2 h). The main reason is that crystalline (Cu) phase and the precipitated intermetallic compound phases cause structure detects, such as

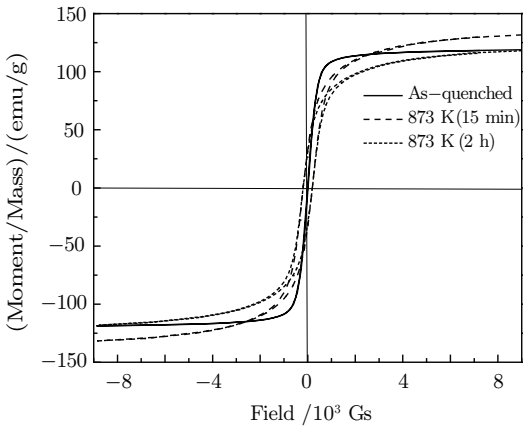


Fig. 5. Magnetic hysteresis loops of the as-quenched and annealed $(Fe_{50}Co_{25}B_{15}Si_{10})_{80}Cu_{20}$ ribbons.

grain boundaries and interfacial defects. These changes in structure lead to the increase of H_c. Once the crystallization process is accomplished, H_c approaches to its maximum. The relaxation of stress in the heating process also has possibly an effect on the change of the magnetic properties.

4. Conclusion

A macroscopic dual-layer structure is formed in the melt-spun $(Fe_{50}Co_{25}B_{15}Si_{10})_{80}Cu_{20}$ alloy ribbon due to metastable liquid phase separation before solidification. There is a clear interface between the Cu-rich and the (Fe, Co)-rich layer. The (Fe, Co)-rich layer is solidified as metallic glass. The hysteresis loops indicate that the coercivity of the ribbon is almost zero in the as-quenched state. The crystallization leads to the increase of coercivity and the decrease of saturation magnetization.

References

[1] Conner R D, Dandliker R B and Johnson W L 1998 *Acta Mater.* **46** 6089

[2] Szuecs F, Kim C P and Johnson W L 2001 *Acta Mater.* **49** 1507

[3] Jiang H C, Zhang W L and Zhang W X 2008 *Chin. Phys. Lett.* **25** 1435

[4] Kong L H, Chen R R and Song T T *J. Mag. Mag. Mater.* **323** 3285

[5] Kundig A A, Ohnuma M, Ping D H, Ohkubo T and Hono K 2004 *Acta Mater.* **52** 2441

[6] Nagase T, Yokoyama A and Umakoshi Y 2010 *J. Alloys Compd.* **494** 295

[7] Munitz A and Abbaschian R 1987 *Metall. Trans.* B **18** 565

[8] Cao C D 2006 *Chin. Phys.* **15** 872

[9] Cao C D, Görler G P, Herlach D M and Wei B 2002 *Mater. Sci. Eng.* A **325** 503

[10] Xu J F and Wei B B 2005 *Acta Phys. Sin.* **54** 3444 (in Chinese)

[11] Kim D I and Abbaschian R 2000 *J. Phase Equilibria* **21** 25

[12] Bamberger M, Munitz A, Kaufman L and Abbaschian R 2002 *Calphad.* **26** 375

[13] Cao C D and Görler G P 2005 *Chin. Phys. Lett.* **22** 482

[14] Cao X G, Guo Z C, Che X Z, Liu P and Yin B 1997 *Int. J. Iron Steel Res.* **4** 27

[15] Yamauchi I, Irie T and Sakaguchi H 2005 *J. Alloys Compd.* **403** 211

[16] Takeshi N and Yukichi U 2010 *Intermetallics* **18** 2136

[17] Lesz S, Nowosielski R, Zajdel A, Kostrubiec B and Stoklosa Z 2007 *Archives of Materials Science and Engineering* **28** 91

[18] Szewieczek D, Tyrlik-Held J and Lesz S 2007 *Journal of Achievements in Materials and Manufacturing Engineering* **24** 87

[19] Inoue A, Makino A and Mizushima T 2000 *J. Mag. Mag. Mater.* **215** 246

[20] Schwarz R B, Shen T D, Harms U and Lillo T 2004 *J. Mag. Mag. Mater.* **283** 223

[21] Myron S, Lausanne C H, Thomas T and Edgar Mclaudealain D 2005 U.S. Patent **6 875 522** B2

[22] Wang G H, Pan H, Ke F J, Xia M F and Bai Y L 2008 *Chin. Phys.* B **17** 259

[23] Yosbizalwa Y, Oguma S and Yamauchi K 1988 *J. Appl. Phys.* **64** 6044

[24] Wang W H, Pan M X and Zhao D Q 2004 *J. Phys.*: *Condens. Matter* **16** 3719